Identifying the spectroscopic modes of multiferroic BiFeO$_3$

Randy S. Fishman,[1] Nobuo Furukawa,[2] Jason T. Haraldsen,[3,4] Masaaki Matsuda,[5] and Shin Miyahara[6]

[1]*Materials Science and Technology Division, Oak Ridge National Laboratory, Oak Ridge, Tennessee 37831, USA*

[2]*Department of Physics and Mathematics, Aoyama Gakuin University, Sagamihara, Kanagawa 229-8558, Japan*

[3]*Theoretical Division, Los Alamos National Laboratory, Los Alamos, New Mexico 87545, USA*

[4]*Center for Integrated Nanotechnologies, Los Alamos National Laboratory, Los Alamos, New Mexico 87545, USA*

[5]*Quantum Condensed Matter Division, Oak Ridge National Laboratory, Oak Ridge, Tennessee 37831, USA*

[6]*Asia Pacific Center for Theoretical Physics, Pohang University of Science and Technology, Pohang, Gyeongbuk 790-784, Korea*

We have identified the modes of multiferroic BiFeO$_3$ measured by THz and Raman spectroscopies. Excellent agreement with the observed peaks is obtained by including the effects of easy-axis anisotropy along the direction of the electric polarization. By distorting the cycloidal spin state, anisotropy splits the $\Psi_{\pm 1}$ mode into peaks at 20 and 21.5 cm^{-1} and activates the lower $\Phi_{\pm 2}$ mode at 27 cm^{-1} ($T = 200$ K). An electromagnon is identified with the upper $\Psi_{\pm 1}$ mode at 21.5 cm^{-1}. Our results also explain recent inelastic neutron-scattering measurements.

PACS number(s): 75.25.−j, 75.30.Ds, 75.50.Ee, 78.30.−j

Multiferroic materials hold tremendous technological promise due to the coupling between the electric polarization and magnetic order. Flipping the moments of a multiferroic storage medium by applying a voltage would not generate Joule heating or require large magnetic fields.[1] Since information that is written electrically could be read magnetically, multiferroic devices would transform both magnetic storage and spintronic technologies.

The few multiferroic materials that have been discovered fall into two classes. In "proper" multiferroics, magnetic order develops at a lower temperature than the ferroelectric polarization;[1] in "improper" multiferroics, the electric polarization is directly coupled to the magnetic state,[2,3] which develops at the same temperature. Although the multiferroic coupling is typically stronger in "improper" multiferroics, practical devices are more likely to be based on "proper" multiferroics such as boracite Ni$_3$B$_7$O$_{13}$I and lodestone Fe$_3$O$_4$ (Ref. 1) due to their higher magnetic transition temperatures. So far, the highest transition temperature of a "proper" multiferroic was found in BiFeO$_3$ with $T_N \approx 640$ K.[4–6] BiFeO$_3$ is the only known multiferroic material with T_N above room temperature.

Before BiFeO$_3$ can be utilized in room-temperature devices, however, it is essential to understand the microscopic mechanisms responsible for its magnetoelectric behavior. Recent inelastic neutron-scattering measurements on single-crystal samples of BiFeO$_3$[7,8] were used to estimate the easy-axis anisotropy K along the polarization direction as well as the Dzyaloshinskii-Moriya (DM) coupling D that induces the long-period cycloidal order with wave vector $\mathbf{Q} = (2\pi/a)(0.5 + \delta, 0.5, 0.5 - \delta)$ and $\delta \approx 0.0045$.[4,9–11] Much more precise estimates for those coupling constants may be obtained from the excitation frequencies obtained from THz[12] and Raman[13–15] spectroscopies. This paper evaluates the frequencies of the spectroscopic modes from a model that includes easy-axis anisotropy and DM interactions. In addition to identifying three of the measured peaks and one higher energy mode, our microscopic model also predicts the mode intensities and the selection rules governing their observation.

Due to the displacement of the Bi^{3+} ions, ferroelectricity appears in rhombohedral BiFeO$_3$ below $T_c \approx 1100$ K.[16] For

the pseudocubic unit cell in Fig. 1 with lattice constant $a \approx 3.96$ Å, cycloidal order develops below T_N with propagation vector $(2\pi/a)(\delta, 0, -\delta)$ along $\mathbf{x}'$ for each $(1,1,1)$ plane.[4–6] Neighboring $(1,1,1)$ planes are coupled by the antiferromagnetic (AF) interaction J_1 between the $S = 5/2$ Fe^{3+} spins. The DM interaction $\mathbf{D}$ along $\mathbf{y}'$ or $[-1,2,-1]$ produces a cycloid with spins in the $(-1,2,-1)$ plane. Easy-axis anisotropy K along $[1,1,1]$, parallel to the polarization $\mathbf{P}$, distorts the cycloid by producing odd harmonics of the fundamental ordering wave vector.[17]

Although T_N is much lower than T_c, the magnetic domain distribution of BiFeO$_3$ can be effectively manipulated by an electric field.[5,6,18] In a magnetic field above 20 T, the transformation of the cycloid to an almost commensurate structure with weak ferromagnetic moment[19] is accompanied by a sharp drop of about 40 nC/cm^2 in the electric polarization.[17,20,21] Therefore, the additional polarization $\mathbf{P}^{\text{ind}}$ observed below T_N is induced by the cycloidal spin state.

The coupling between the cycloid and electric polarization is produced by the inverse DM mechanism[22–24] with induced polarization $\mathbf{P}^{\text{ind}} \propto \mathbf{e}_{ij} \times (\mathbf{S}_i \times \mathbf{S}_j)$ where $\mathbf{e}_{ij} = \mathbf{R}_j - \mathbf{R}_i$ and $\mathbf{S}_i$ are the Fe^{3+} spins. Within each $(1,1,1)$ plane, $\mathbf{e}_{ij} = \sqrt{2}a\mathbf{x}'$ connects spins at $\mathbf{R}_i$ and $\mathbf{R}_j = \mathbf{R}_i + \sqrt{2}a\mathbf{x}'$. So $\mathbf{S}_i \times \mathbf{S}_j$ points along $\mathbf{y}'$ and $\mathbf{P}^{\text{ind}}$ points along $\mathbf{z}'$.

The spin-wave (SW) excitations of BiFeO$_3$ may be evaluated from the Hamiltonian[25]

$$H = J_1 \sum_{\langle i,j \rangle} \mathbf{S}_i \cdot \mathbf{S}_j + J_2 \sum_{\langle i,j \rangle'} \mathbf{S}_i \cdot \mathbf{S}_j - K \sum_i (\mathbf{S}_i \cdot \mathbf{z}')^2$$
$$- D \sum_{\mathbf{R}_j = \mathbf{R}_i + \sqrt{2}a\mathbf{x}'} \mathbf{y}' \cdot (\mathbf{S}_i \times \mathbf{S}_j). \qquad (1)$$

In the first and second exchange terms, $\langle i, j \rangle$ denotes a sum over nearest neighbors and $\langle i, j \rangle'$ a sum over next-nearest neighbors. The third term originates from the easy-axis anisotropy along $\mathbf{z}'$ and the fourth term from the DM interaction with $\mathbf{D}$ along $\mathbf{y}'$. For a fixed cycloidal period, D is a smoothly increasing function of K, as shown in Fig. 5 of Ref. 8. This is the minimum model required to understand the excitation spectrum of BiFeO$_3$. Whereas J_1 and J_2 determine the high-frequency part of the SW spectrum, which extends above 70 meV,[7,8] K and
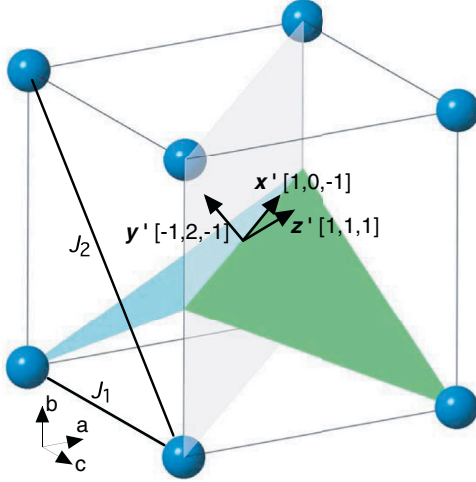
FIG. 1. (Color online) The pseudocubic unit cell for BiFeO$_3$ showing $\mathbf{x'}$, $\mathbf{y'}$, and $\mathbf{z'}$ directions. The distorted spin spiral propagates along the $\mathbf{x'}$ direction with spins in the $(-1,2,-1)$ plane. AF interactions J_1 and J_2 are also indicated.

FIG. 2. (Color online) The SW modes of BiFeO$_3$ versus q/δ for wave vector $(2\pi/a)(0.5 + q, 0.5, 0.5 - q)$. Dashed lines show all possible excitations and the solid lines show only those modes with nonzero intensity. (a) For $K = 0$, two of the three SW branches are plotted versus q/δ in the inset with points Φ_n and Ψ_n at multiples of δ for $c = 1$. The solid (green) point at Ψ_1 indicates a MR and EM mode. (b) For $K = 0.002$ meV, the $\Psi_{\pm 1}$ mode (green and blue) splits and the lower $\Phi_{\pm 2}$ mode (red) is activated. The x' (blue), y' (red), and z' (green) components of the MR modes are indicated. The EM mode corresponds to the upper (blue) $\Psi_{\pm 1}$ mode.

D are required to explain the low-frequency SW gaps and spectroscopic modes.

Since $\delta = 0.0045$ is close to $1/222$, a unit cell containing 222 sites within each of two neighboring $(1,1,1)$ planes was used to characterize the distorted cycloid. The cycloid was expanded in odd harmonics of the fundamental wave vector $\mathbf{Q} = (2\pi/a)(0.5 + \delta, 0.5, 0.5 - \delta)$:[26]

$$S_{z'}(\mathbf{R}) = S \sum_{m=0}^{\infty} C_{2m+1} \cos[((2m+1)\mathbf{Q} \cdot \mathbf{R}], \quad (2)$$

$$S_{x'}(\mathbf{R}) = \sqrt{S^2 - S_{z'}(\mathbf{R})^2} \, \mathrm{sgn}[\sin(\mathbf{Q} \cdot \mathbf{R})], \quad (3)$$

where the odd-order coefficients C_{2m+1} satisfy $\sum_{m=0}^{\infty} C_{2m+1} = 1$.

Excitation frequencies and intensities were evaluated by performing a $1/S$ expansion in the rotated frame of reference for each spin[27] in the 444-site unit cell with two AF-coupled layers. Although there are 444 positive eigenfrequencies for each wave vector, only a handful of those frequencies have nonzero intensity. Frequencies and intensities are evaluated using the AF interactions $J_1 = 4.5$ meV and $J_2 = 0.2$ meV, which describe the inelastic neutron-scattering measurements[7,8] at 200 K.[28] Below 4 meV and for $0 \leqslant q < 2\delta$, all possible SW frequencies are denoted by the dashed curves in Fig. 2 for $K = 0$ and 0.002 meV. Branches with nonzero intensity are indicated by the dark solid curves.

When $K = 0$, two of the three SW branches are plotted in the inset to Fig. 2(a) with points at multiples of the wave vector $q = \delta$ labeled as Φ_n or Ψ_n. For small frequencies and $q = n\delta$, $\omega(\Phi_{n-1}) = |n-1| c\delta$ and $\omega(\Psi_n) = \sqrt{1 + n^2} c\delta$, where c is the SW velocity of the linear branches.[29] In the reduced-zone scheme, odd-n Ψ_n and even-n Φ_n modes lie at $q = \delta$ while even-n Ψ_n and odd-n Φ_n modes lie at $q = 0$.

When $K > 0$, the SW spectrum at small frequencies changes dramatically. Higher harmonics of the cycloid split every set of crossing $\Phi_{\pm n}$ and $\Psi_{\pm n}$ modes. The largest splitting occurs at $q = 0$ between the $\Phi_{\pm 1}$ modes. A smaller splitting
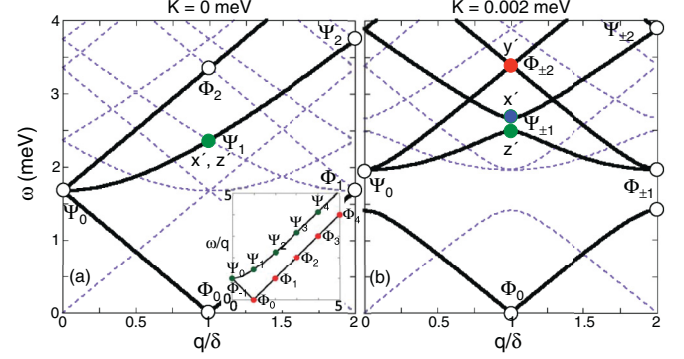
occurs at $q = \delta$ between the $\Psi_{\pm 1}$ modes. While the Φ_0 mode is shifted slightly above zero frequency, the Ψ_0 mode is moved up to just below the top $\Phi_{\pm 1}$ mode. Figure 3 plots the evolution of those points with anisotropy. Although too small to appear in this plot, even the $\Phi_{\pm 2}$ modes are split by anisotropy. Previous efforts[13,15] to identify the spectroscopic modes of BiFeO$_3$ based on the Φ_n and Ψ_n mode frequencies with $K = 0$ failed to account for these mode splittings.

Spectroscopic intensities are given by the matrix elements of $M_\alpha = g\mu_B \sum_i S_{i\alpha}$ for magnetic resonance (MR) and by the
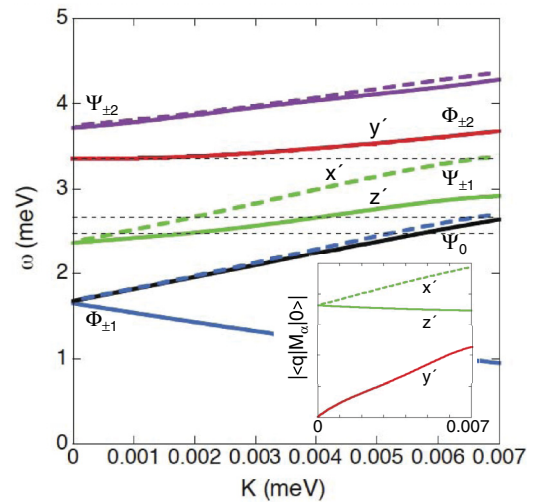

FIG. 3. (Color online) The evolution of the SW frequencies with easy-axis anisotropy. Solid and dashed pairs of curves indicate split $\pm n$ modes. Inset shows the matrix elements for the MR modes (arbitrary units) versus K. The horizontal dashed lines indicate the experimental results of Ref. 12 at 200 K.

matrix elements of the induced polarization

$$P_\alpha^{\text{ind}} = \lambda \sum_{\mathbf{R}_j = \mathbf{R}_i + \sqrt{2}a\mathbf{x}'} \{\mathbf{x}' \times (\mathbf{S}_i \times \mathbf{S}_j)\}_\alpha \qquad (4)$$

for the electromagnon (EM).[30] Each matrix element is evaluated between the ground state $|0\rangle$ and an excited state $|q\rangle$ containing a single magnon with cycloidal wave vector $q = \delta$. Details about how to evaluate those matrix elements are provided in the Supplemental Material.[31]

When $K = 0$, there is a single MR peak at the Ψ_1 point in Fig. 2(a). For this mode, $|\langle\delta|M_{x'}|0\rangle| = |\langle\delta|M_{z'}|0\rangle| > 0$ and $|\langle\delta|M_{y'}|0\rangle| = 0$. An EM peak with component y' coincides with the MR peak. Only the y' component of $\langle\delta|P_\alpha^{\text{ind}}|0\rangle$ is nonzero. No other frequencies at $q = \delta$ are magnetoelectrically active for $K = 0$.

When $K > 0$, both $\Psi_{\pm 1}$ modes are active with nonzero x' and z' MR matrix elements for the upper and lower modes, respectively. The MR matrix elements $|\langle\delta|M_\alpha|0\rangle|$ of those modes are plotted versus anisotropy in the inset to Fig. 3. While the matrix element of the lower $\Psi_{\pm 1}$ mode decreases with anisotropy, that of the upper $\Psi_{\pm 1}$ mode increases. Because the third harmonic of the $\Psi_{\pm 1}$ modes couples to the first harmonic of the $\Phi_{\pm 2}$ modes, the lower $\Phi_{\pm 2}$ mode is activated by anisotropy[29] with a nonzero y' MR matrix element plotted in the inset to Fig. 3.

A large EM peak with matrix element $\langle\delta|P_{y'}^{\text{ind}}|0\rangle$ coincides with the upper $\Psi_{\pm 1}$ mode. Another EM peak with matrix element about 10 times smaller was found at the upper $\Psi_{\pm 3}$ mode with frequency 5.39 meV (43.4 cm^{-1}). This peak also has a significant MR matrix element $|\langle\delta|M_{x'}|0\rangle|$. Hence, the active $\Psi_{\pm(2m+1)}$ peaks correspond to out-of-plane modes of the cycloid (excited by magnetic fields along $\mathbf{x}'$ or $\mathbf{z}'$) while the active $\Phi_{\pm 2m}$ peaks correspond to in-plane modes of the cycloid (excited by a magnetic field along $\mathbf{y}'$).

Below 30 cm^{-1}, THz spectroscopy[12] observed four infrared modes with frequencies (measured at or extrapolated to 200 K[28]) of 17.5, 20, 21.5, and 27 cm^{-1}. The upper three mode frequencies are denoted by the dashed lines in Fig. 3. These modes can be quite accurately described by $K = 0.002$ meV, which produces MR peaks at 2.49, 2.67, and 3.38 meV, remarkably close to the observed peaks at 2.48, 2.67, and 3.35 meV. Talbayev *et al.*[12] conjectured that the 20 and 21.5 cm^{-1} lines were produced by the splitting of the $\Psi_{\pm 1}$ modes due to a modulated DM interaction along $\mathbf{z}'$. We conclude that the splitting of the $\Psi_{\pm 1}$ modes is caused by easy-axis anisotropy along $\mathbf{z}'$ with quantitatively accurate values. Perhaps due to the small matrix element plotted in the inset to Fig. 3, the lower $\Phi_{\pm 2}$ peak at 27 cm^{-1} was not detected[12] above about 150 K.

The selection rules governing the MR modes also agree with the results of Ref. 12. Field directions $\mathbf{h}_1\|[1,-1,0]$ and $\mathbf{h}_2\|[1,1,0]$ can be written as $\mathbf{h}_1 = \mathbf{x}'/2 - \sqrt{3}\mathbf{y}'/2$ and $\mathbf{h}_2 = \mathbf{x}'/2 + \sqrt{3}\mathbf{y}'/6 + \sqrt{2/3}\mathbf{z}'$. Consequently, the lower $\Phi_{\pm 2}$ mode with MR component y' and the upper $\Psi_{\pm 1}$ mode with MR component x' are excited both by fields $\mathbf{h}_1$ and $\mathbf{h}_2$, but the lower $\Psi_{\pm 1}$ mode with MR component z' is only excited by field $\mathbf{h}_2$.[32] The predicted upper $\Psi_{\pm 3}$ mode with MR component x' should be excited by both fields $\mathbf{h}_1$ and $\mathbf{h}_2$.

Since it is associated with a large EM peak, the upper $\Psi_{\pm 1}$ mode can also be excited by an electric field along $\mathbf{y}'$. The observation of nonreciprocal directional dichroism (NDD) under an external magnetic field $\mathbf{B}^{\text{ex}}$ along $\mathbf{z}'$[30] would confirm this prediction. NDD requires linearly polarized electromagnetic waves propagating along $\mathbf{x}'$ with electric and magnetic components $\mathbf{E}^\omega\|\mathbf{y}'$ and $\mathbf{H}^\omega\|\mathbf{z}'$.

By contrast, the observed low-energy mode at frequency 17.5 cm^{-1} (2.17 meV) cannot be explained by our model because there are no zone-center excitations below the lower $\Psi_{\pm 1}$ mode at 2.5 meV. Nevertheless, the 2.17 meV peak lies tantalizingly close to both the upper $\Phi_{\pm 1}$ mode and the Ψ_0 mode at $q = 0$ in Fig. 2(b). It is possible that the 2.17 meV peak is associated with a more complex magnetic structure induced by some interaction or anisotropy not included in our model. Additional long-range order with wave vector $(2\pi/a)(\delta, 0, -\delta)$ or $(2\pi/a)(0.5, 0.5, 0.5)$ would hybridize the $\Phi_{\pm 1}$ or Ψ_0 modes at $q = 0$ with the $\Psi_{\pm 1}$ modes at $q = \delta$. In Raman spectroscopy, the anomalies of the 2.17 meV peak at 140 K and 200 K were identified with spin reorientations[13,14] of the cycloid. However, any such spin reorientation must respect the selection rules for the zone-center MR modes.

All of the active zone-center modes have been observed with Raman spectroscopy.[13–15] The Raman peak[15] at 23 cm^{-1} ($T = 10$ K) detected with parallel polarizations (exciting out-of-plane modes) can be identified with the $\Psi_{\pm 1}$ modes and the 25.5 cm^{-1} peak detected with crossed polarizations (exciting in-plane modes) can be identified with the lower $\Phi_{\pm 2}$ mode. Another Raman peak[14] at 43.4 cm^{-1} ($T = 80$ K) lies quite near the estimated frequency of the upper $\Psi_{\pm 3}$ mode.

Governed by different selection rules than THz spectroscopy, Raman spectroscopy also observed several $q = 0$ cycloidal modes. These include strong peaks at 34.5 cm^{-1} (4.28 meV, $T = 80$ K)[14] and 32 cm^{-1} (3.96 meV, $T = 10$ K),[15] close to the predicted energy of the $\Psi_{\pm 2}$ modes. As conjectured above, additional long-range order may produce such $q = 0$ cycloidal peaks in the Raman spectrum.

Earlier estimates for K and D were based on low-energy inelastic neutron-scattering measurements taken at the wave vector $(2\pi/a)(0.5, 0.5, 0.5)$.[8] Because the inelastic-scattering cross section is quite broad, estimates based on those measurements are not as precise as the estimates given above based on spectroscopy measurements. By using the predicted frequencies of the $\Phi_{\pm 1}$ modes to match the primary inelastic peaks at 1.1 and 2.5 meV, Matsuda *et al.* estimated that $K \approx 0.005$ meV.[28] However, peaks in the inelastic intensity $\chi''(\omega)$ may be slightly shifted away from those frequencies due to the finite resolution of the measurements.

Averaged over a realistic resolution function and including the three sets of twins states with wave vectors along $\mathbf{x}'$, $\mathbf{y}'$, and $\mathbf{z}'$, $\chi''(\omega)$ is plotted in Fig. 4 for six values of K from 0 to 0.005 meV. The inset provides the inelastic measurements at 200 K, which are almost temperature independent between 100 and 300 K.[33] For $K > 0$, the lowest two peaks are near the $q = 0$, $\Phi_{\pm 1}$ modes. Due to the instrumental resolution, the $q = \delta$, $\Psi_{\pm 1}$, and $\Phi_{\pm 2}$ modes appear as two peaks in $\chi''(\omega)$.

The best qualitative agreement with the inelastic measurements is obtained with $K \approx 0.004$ meV. Below 5 meV, the measured $\chi''(\omega)$ contains peaks at 1.2, 2.4, 3.4, and 4.4 meV.
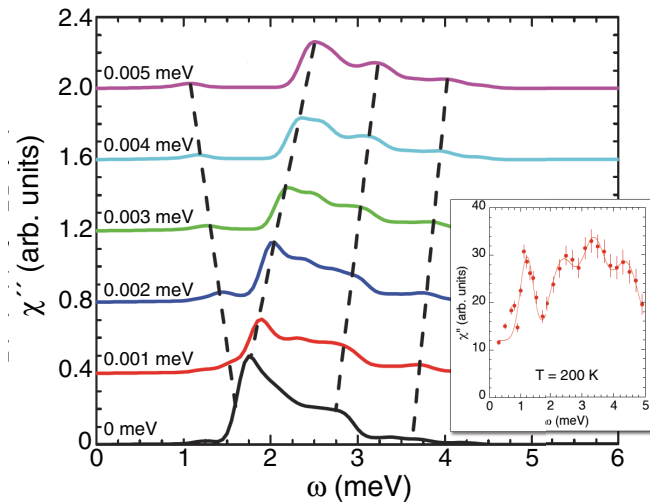
FIG. 4. (Color online) The averaged neutron-scattering intensity χ'' at $(2\pi/a)(0.5,0.5,0.5)$ versus ω for K from 0 to 0.005 meV. Measurements at $T = 200$ K in the inset (Ref. 33).

While four nearby peaks are predicted by our model, the lowest-energy peak is too weak and the two highest-energy peaks are slightly too low compared to the experimental results.

A value for K between 0.002 and 0.004 meV is consistent with the prediction $K = 0.0027$ meV obtained from Monte-Carlo simulations of the phase diagram in a magnetic field.[19] As discussed above, anisotropy produces higher harmonics $C_{2m+1>1}$ of the cycloid. Within the predicted range of K, $624 > (C_1/C_3)^2 > 176$. Elastic neutron-scattering[9] and NMR measurements[34] indicate that $I_1/I_3 = (C_1/C_3)^2$ is given by 500 and 25, respectively. However, the third harmonic in the

NMR measurement may be enhanced by the high ^{57}Fe isotope content of the sample.[35] Because more precise estimates are provided by THz and Raman spectroscopies, a value for K closer to the lower limit of 0.002 meV and a value for $(C_1/C_3)^2$ closer to 500 is likely.

To conclude, our microscopic model identifies three of the peaks measured by THz and Raman spectroscopies. Our work suggests that the observed low-energy peak is produced by a distortion that couples $q = 0$ and $q = \delta$ modes. The single fitting parameter of this model, the easy-axis anisotropy, can be determined independently by accurately measuring the spin harmonics of the cycloid. Unlike previous assignments of the spectroscopic modes, our work properly accounts for the splitting and activation of the $q = \delta$ modes by anisotropy. The pertinent features of the mode spectrum discussed in this paper should also be found in other materials with distorted cycloidal order. Ultimately, we hope that understanding the microscopic interactions in $BiFeO_3$ will hasten their applications in room-temperature devices.

[1] W. Eerenstein, N. D. Mathur, and J. F. Scott, Nature (London) **442**, 759 (2006).

[2] D. I. Khomskii, Magn. Magn. Mater. **306**, 1 (2006).

[3] S.-W. Cheong and M. Mostovoy, Nat. Mater. **6**, 13 (2007).

[4] I. Sosnowska, T. Peterlin-Neumaier, and E. Steichele, J. Phys. C **15**, 4835 (1982).

[5] D. Lebeugle, D. Colson, A. Forget, M. Viret, A. M. Bataille, and A. Gukasov, Phys. Rev. Lett. **100**, 227602 (2008).

[6] S. Lee, W. M. Ratcliff II, S.-W. Cheong, and V. Kiryukhin, Appl. Phys. Lett. **92**, 192906 (2008).

[7] J. Jeong, E. A. Goremychkin, T. Guidi, K. Nakajima, G. S. Jeon, S.-A. Kim, S. Furukawa, Y. B. Kim, S. Lee, V. Kiryukhin, S.-W. Cheong, and J.-G. Park, Phys. Rev. Lett. **108**, 077202 (2012).

[8] M. Matsuda, R. S. Fishman, T. Hong, C. H. Lee, T. Ushiyama, Y. Yanagisawa, Y. Tomioka, and T. Ito, Phys. Rev. Lett. **109**, 067205 (2012).

[9] M. Ramazanoglu, W. Ratcliff II, Y. J. Choi, S. Lee, S.-W. Cheong, and V. Kiryukhin, Phys. Rev. B **83**, 174434 (2011).

[10] J. Herrero-Albillos, G. Catalan, J. A. Rodriguez-Velamazan, M. Viret, D. Colson, and J. F. Scott, J. Phys.: Condens. Matter **22**, 256001 (2010).

[11] I. Sosnowska and R. Przenioslo, Phys. Rev. B **84**, 144404 (2011).

[12] D. Talbayev, S. A. Trugman, S. Lee, H. T. Yi, S.-W. Cheong, and A. J. Taylor, Phys. Rev. B **83**, 094403 (2011).

[13] M. Cazayous, Y. Gallais, A. Sacuto, R. de Sousa, D. Lebeugle, and D. Colson, Phys. Rev. Lett. **101**, 037601 (2008).

[14] M. K. Singh, R. S. Katiyar, and J. F. Scott, J. Phys.: Condens. Matter **20**, 252203 (2008).

[15] P. Rovillain, M. Cazayous, Y. Gallais, A. Sacuto, R. P. S. M. Lobo, D. Lebeugle, and D. Colson, Phys. Rev. B **79**, 180411(R) (2009).

[16] J. R. Teague, R. Gerson, and W. J. James, Solid State Commun. **8**, 1073 (1970).

[17] A. M. Kadomtseva, A. K. Zvezdin, Yu. F. Popv, A. P. Pyatakov, and G. P. Vorob'ev, JTEP Lett. **79**, 571 (2004).

[18] S. Lee, T. Choi, W. Ratcliff II, R. Erwin, S.-W. Cheong, and V. Kiryukhin, Phys. Rev. B **78**, 100101(R) (2008).

[19] K. Ohoyama, S. Lee, S. Yoshii, Y. Narumi, T. Morioka, H. Nojiri, G. S. Jeon, S.-W. Cheong, and J.-G. Park, J. Phys. Soc. Jpn. **80**, 125001 (2011).

[20] J. Park, S.-H. Lee, S. Lee, F. Gozzo, H. Kimura, Y. Noda, Y. J. Choi, V. Kiryukhin, S.-W. Cheong, Y. Jo, E. S. Choi, L. Balicas, G. S. Jeon, and J.-G. Park, J. Phys. Soc. Jpn. **80**, 114714 (2011).

[21] M. Tokunaga, M. Azuma, and Y. Shimakawa, J. Phys. Soc. Jpn. **79**, 064713 (2010).

[22]H. Katsura, N. Nagaosa, and A. V. Balatsky, Phys. Rev. Lett. **95**, 057205 (2005).

[23]M. Mostovoy, Phys. Rev. Lett. **96**, 067601 (2006).

[24]I. A. Sergienko and E. Dagotto, Phys. Rev. B **73**, 094434 (2006).

[25]I. Sosnowska and A. K. Zvezdin, J. Magn. Magn. Mater. **140–144**, 167 (1995).

[26]R. S. Fishman and S. Okamoto, Phys. Rev. B **81**, 020402(R) (2010).

[27]J. T. Haraldsen and R. S. Fishman, J. Phys.: Condens. Matter **21**, 216001 (2009).

[28]To account for the suppression of the observed moment at 200 K, Ref. 8 took $2\mu_B\sqrt{S(S+1)} = 4.11\mu_B$ to be about 30% lower than its value with $S = 5/2$. Here we take $2\mu_B\sqrt{S(S+1)} = 5.92\mu_B$ and reduce the exchange interactions accordingly. So the estimates $J_1 = 6.48$ meV, $J_2 = 0.29$ meV, $K = 0.0068$ meV, and $D = 0.162$ meV from Ref. 8 are equivalent to $J_1 = 4.5$ meV, $J_2 = 0.2$ meV, $K = 0.005$ meV, and $D = 0.119$ meV in this paper.

[29]R. de Sousa and J. E. Moore, Phys. Rev. B **77**, 012406 (2008).

[30]S. Miyahara and N. Furukawa, J. Phys. Soc. Jpn. **81**, 023712 (2012).

[31]See Supplemental Material at http://link.aps.org/supplemental/10.1103/PhysRevB.86.220402 for a brief description of the method used to evaluate the MR and EM matrix elements.

[32]In a crystal with $\mathbf{P}\|\mathbf{z}'$, there are three possible orientations of $\mathbf{Q}$. The selection rules indicate that either $(0.5 + \delta, 0.5, 0.5 - \delta)$ or $(0.5, 0.5 - \delta, 0.5 + \delta)$ is realized in Ref. 12 since the upper $\Psi_{\pm 1}$ mode would be inactive in field $\mathbf{h}_2$ for a cycloid with $(0.5 - \delta, 0.5 + \delta, 0.5)$.

[33]These data were obtained by M. Matsuda at the Cold Triple-Axis Neutron Spectrometer (CTAX) installed at the High-Flux Isotope Reactor (HFIR) of Oak Ridge National Laboratory. The scattering intensities are converted to χ'' by multiplying by $1 - \exp(-\hbar\omega/kT)$.

[34]A. V. Zalesskii, A. K. Zvezdin, A. A. Frolov, and A. A. Bush, JETP Lett. **71**, 465 (2000); A. V. Zalesskii, A. A. Frolov, A. K. Zvezdin, A. A. Gippius, E. N. Morozova, D. F. Khozeev, A. S. Bush, and V. S. Pokatilov, JETP **95**, 101 (2002).

[35]S. Pokatilov and A. S. Sigov, JETP **110**, 440 (2010).